View metadata, citation and similar papers at core.ac.uk

brought to you by CORE

provided by Ghent University Academic Bibliography

European Heart Journal – Cardiovascular Imaging
doi:10.1093/ehjci/jev346

Targeting of vascular cell adhesion molecule-1 by ^{18}F-labelled nanobodies for PET/CT imaging of inflamed atherosclerotic plaques

Gezim Bala[1,2]*, Anneleen Blykers[2], Catarina Xavier[2], Benedicte Descamps[3], Alexis Broisat[4], Catherine Ghezzi[4], Daniel Fagret[4], Guy Van Camp[2], Vicky Caveliers[2,5], Christian Vanhove[3], Tony Lahoutte[2,5], Steven Droogmans[1,2], Bernard Cosyns[1,2], Nick Devoogdt[2], and Sophie Hernot[2]

[1]Centrum voor Hart-en Vaatziekten (CHVZ), UZ Brussel, Brussels, Belgium; [2]In Vivo Cellular and Molecular Imaging (ICMI), Faculty of Medicine and Pharmacy, Vrije Universiteit Brussel (VUB), Laarbeeklaan 103, Brussels B-1090, Belgium; [3]iMinds-IBiTech-MEDISIP, Department of Electronics and Information Systems, Universiteit Gent, Ghent, Belgium; [4]Radiopharmaceutiques Biocliniques, INSERM, 1039—Université de Grenoble, La Tronche, France; and [5]Nuclear Medicine Department, UZ Brussel, Brussels, Belgium

Received 21 August 2015; accepted after revision 12 December 2015

Aims Positron emission tomography–computed tomography (PET-CT) is a highly sensitive clinical molecular imaging modality to study atherosclerotic plaque biology. Therefore, we sought to develop a new PET tracer, targeting vascular cell adhesion molecule (VCAM)-1 and validate it in a murine atherosclerotic model as a potential agent to detect atherosclerotic plaque inflammation.

Methods and results The anti-VCAM-1 nanobody (Nb) (cAbVCAM-1–5) was radiolabelled with Fluorine-18 (^{18}F), with a radiochemical purity of >98%. *In vitro* cell-binding studies showed specific binding of the tracer to VCAM-1 expressing cells. *In vivo* PET/CT imaging of ApoE$^{-/-}$ mice fed a Western diet or control mice was performed at 2h30 post-injection of [^{18}F]-FB-cAbVCAM-1–5 or ^{18}F-control Nb. Additionally, plaque uptake in different aorta segments was evaluated *ex vivo* based on extent of atherosclerosis. Atherosclerotic lesions in the aortic arch of ApoE$^{-/-}$ mice, injected with [^{18}F]-FB-anti-VCAM-1 Nb, were successfully identified using PET/CT imaging, while background signal was observed in the control groups. These results were confirmed by *ex vivo* analyses where uptake of [^{18}F]-FB-cAbVCAM-1–5 in atherosclerotic lesions was significantly higher compared with control groups. Moreover, uptake increased with the increasing extent of atherosclerosis (Score 0: 0.68 ± 0.10, Score 1: 1.18 ± 0.36, Score 2: 1.49 ± 0.37, Score 3: 1.48 ± 0.38%ID/g, Spearman's $r^2 = 0.675$, $P < 0.0001$). High lesion-to-heart, lesion-to-blood, and lesion-to-control vessel ratios were obtained (12.4 ± 0.4, 3.3 ± 0.4, and 3.1 ± 0.6, respectively).

Conclusion The [^{18}F]-FB-anti-VCAM-1 Nb, cross-reactive for both mouse and human VCAM-1, allows non-invasive PET/CT imaging of VCAM-1 expression in atherosclerotic plaques in a murine model and may represent an attractive tool for imaging vulnerable atherosclerotic plaques in patients.

Keywords atherosclerosis • VCAM-1 • nanobody • molecular imaging • PET/CT

Downloaded from by guest on January 26, 2016

Introduction

Many data support a crucial role of inflammation in the development and progression of atherosclerosis.[1,2] Moreover, inflammation is involved in plaque destabilization and promotes thrombus formation.[1] Indeed, post-mortem studies, related to acute coronary events, reveal extensive infiltration of inflammatory cells in culprit lesions.[3] Vascular cell adhesion molecule-1 (VCAM-1), expressed on endothelial cells, plays an important role in the disease progression by attracting inflammatory cells (monocytes and T-lymphocytes) to the developing lesion.[4] In advanced lesions, VCAM-1 is also expressed at the level of neovessels and may reflect the ongoing inflammation

* Corresponding author. Tel: +32 2 477 49 91; Fax: +32 2 477 50 17. E-mail: gezim.bala@vub.ac.be

Published on behalf of the European Society of Cardiology. All rights reserved. © The Author 2016. For permissions please email: journals.permissions@oup.com.

within the plaque.[5] These properties make VCAM-1 an attractive target for the molecular imaging of inflammation in atherosclerosis.[6]

Nanobodies (Nbs) are the smallest antigen-binding fragments (12–15 kDa) that are derived from heavy-chain-only antibodies naturally occurring in camelids.[7] Their small size, nanomolar-range affinities, high specificity, and fast blood clearance make them appealing ligands for molecular imaging approaches[8] and this has been shown for several experimental disease models.[9–16] Moreover, a Phase I clinical trial demonstrated the applicability of Nb-based tracers in humans.[17]

Nuclear imaging techniques are the modalities of choice for molecular imaging because of their high sensitivity. We have recently reported the use of a technetium-99 m (^{99m}Tc)-labelled anti-VCAM-1 Nb, referred to as cAbVCAM-1–5, as strategy for the detection of inflamed atherosclerotic plaque with single-photon emission computed tomography (SPECT).[10] Yet, positron emission tomography (PET) is more appropriate for clinical use compared with SPECT because of its superior spatial resolution (3–5 vs. 10–15 mm), higher sensitivity (0.8 vs. 0.001%), and more accurate quantification.[18] Despite the advantages of PET, only a few clinical studies regarding molecular imaging of inflammation in atherosclerosis have been conducted. They are predominantly performed with tracers, e.g. ^{18}F-FDG,[15] ^{11}C-PK11195,[19] or ^{18}F-FLT.[20] However, approaches using ^{18}F-FDG or ^{11}C-PK11195 are limited to the imaging of noncoronary atherosclerosis because of tracer uptake in the myocardium.[19,21,22] Therefore, the development of new robust PET tracers for imaging of biological processes implicated in high-risk atherosclerotic plaques is still warranted.

In the current study, our objective is to generate a PET analogue of anti-VCAM-1 Nb for PET/CT imaging of atherosclerosis as a further step to clinical translation. Specifically, we describe (i) the radiolabeling of cAbVCAM-1–5 with ^{18}F, (ii) the assessment of the functionality and specific targeting of this tracer, and (iii) *in vivo* PET/CT imaging of atherosclerotic lesions in apolipoprotein-deficient (ApoE$^{-/-}$) mice.

Methods

^{18}F-Radiolabelling of cAbVCAM-1–5 nanobody

Nanobodies recognizing both mouse and human VCAM-1 homologues have been described previously. Herein, a lead compound, cAbVCAM-1–5, was selected as best candidate for further studies.[10] *N*-Succinimidyl-4-[^{18}F]fluorobenzoate ([^{18}F]-SFB) synthesis consisted of a three-step, one-pot reaction by solid-phase extraction (SPE) purification as described previously.[23] The [^{18}F]-SFB synthesis was incorporated into a commercially available synthetic module (SynthERA® module, IBA Molecular, Belgium). Coupling of dry [^{18}F]-SFB with cAbVCAM-1–5 Nb was performed in borate buffer (0.1 M, pH 8.5, 300 μL, 18.5 nmol Nb) for 20 min at room temperature, and the labelling mixture was purified using a PD-10 column (GE Healthcare, Belgium). The radiochemical identity and purity were assessed by size-exclusion chromatography (SEC, Superdex 75, 5/150 GL, GE Healthcare, PBS 0.3 mL min^{-1}) and by reverse-phase high-performance liquid chromatography (RP-HPLC). For the latter, a polystyrene divinylbenzene copolymer reversed-phase column (PLRP-S 300 Å, 5 μm, 250/4 mm, Agilent) was used applying the following gradient (A: 0.1% TFA in water; B: 0.1% TFA in acetonitrile): 0–5 min 25% B, 5–7 min 25–34% B, 7–10 min 34–100% B, and 10–25 min 100% B at a flow rate of 1 mL min^{-1}. To evaluate the stability *in vitro*, [^{18}F]FB-cAbVCAM-1–5 Nb was incubated in phosphate-buffered saline (PBS) or human serum for 3 h and analysed by RP-HPLC or SEC. Additionally, urine and serum samples were obtained after intravenous injection of [^{18}F]FB-cAbVCAM-1–5 and analysed by SEC.

In vitro assessment of functionality and specificity

The functionality of [^{18}F]FB-anti-VCAM-1 Nb was assessed by cell-binding studies using the mouse endothelial cell line bEND5 (ECACC). These cells were stimulated with 10 ng/mL tumour necrosis factor-alpha (TNF-α) for 18 h to induce VCAM-1 expression. Five nanomolars of [^{18}F]FB-cAbVCAM-1–5 was incubated during 1.5 h at 37°C. After removal of unbound tracer, the bound fraction was collected and counted in a gamma-counter (Canberra-Packard, Downers Grove, IL, USA). Non-stimulated cells were used as negative control. Competition binding studies with a 300-fold molar excess of unlabelled Nb were performed to show the specificity of the binding. Experiments were performed in triplicate. The results were normalized to the TNFα-negative condition.

Animal model

The animal study protocol was approved by the ethical committee for animal research of the Vrije Universiteit Brussel. Female (5-week-old) ApoE$^{-/-}$ mice (Charles-River, L'Arbresle, France) were fed a Western diet (D12108C, Research Diets, New Brunswick, NJ, USA) for 21–25 weeks to induce atherosclerotic lesions. Lesions develop all along the aorta, but are most prevalent in the region of the ascending aorta and aortic arch. Female healthy control C57Bl/6 mice (Charles-River) were used as control mice and remained on a standard chow diet.

Ex vivo biodistribution and atherosclerotic lesion uptake

ApoE$^{-/-}$ mice ($n = 6$) and C57Bl/6 ($n = 6$) control mice were injected intravenously with [^{18}F]FB-cAbVCAM-1–5 Nb (5–10 μg/7.1 ± 1.7 MBq). To demonstrate the specific uptake of the Nb, additional ApoE$^{-/-}$ mice were injected with ^{18}F-labelled non-targeting control Nb ([^{18}F]FB-cAbBCII-10)[10] ($n = 6$) or with 70-fold molar excess of unlabelled cAbVCAM-1–5 Nb ($n = 6$). Mice were sacrificed at 3 h post-injection. Organs and tissues of interest were dissected, weighed and counted against a standard of known activity. Tissue or organ uptake was calculated and expressed as percentage of injected dose per gram (%ID/g), corrected for decay. Additional biodistribution data in C57Bl/6 mice at earlier time points are added as Supplementary data.

To assess atherosclerotic lesion uptake, the aorta was dissected from aortic root to iliac bifurcation and was cut into 8–10 segments. The segments were analysed on a microscope and a lesion-extension score was given according to plaque content: (Score 0) no lesion, (Score 1) lesion covering up to 30% of the segment, (Score 2) lesions covering 30–75% of the segment, and (Score 3) lesions extending over the whole segment. Each segment was then weighed and counted for radioactivity in the gamma-counter. Lesion-to-blood and lesion-to-heart ratios were also determined. The 'lesion' and 'control lesion' were defined as the aorta segment with lesions extending over the whole segment length (Score 3) and aorta segment with no atherosclerosis development (Score 0), respectively.

Downloaded from by guest on January 26, 2016

PET/CT imaging

In vivo imaging was performed on a FLEX Triumph II triple-modality system (TriFoil Imaging, Chatsworth, CA 91311, USA). Four groups of animals were scanned ($n = 3$ per group): C57Bl/6 control mice, ApoE$^{-/-}$ mice, ApoE$^{-/-}$ mice injected with non-targeting control Nb, and ApoE$^{-/-}$ mice injected with 70-fold molar excess of unlabelled Nb. One hundred and fifty minutes after tracer injection (4.68 ± 2.45 MBq), the animals were placed under general anaesthesia using 2–5% isoflurane, and a 30-min PET scan was acquired. The PET images were reconstructed into a 200 × 200 × 63 matrix by a 2D maximum likelihood expectation maximization (MLEM) algorithm (LabPET Version 1.12.1, TriFoil Imaging, Chatsworth, CA, USA) using 60 iterations and a voxel size of 0.5 × 0.5 × 1.175 mm^3 (x, y, z). Each PET scan was followed by a CT scan using the following acquisition parameters: 256 projections, detector pixel size 50 μm, tube voltage 75 kV, tube current 500 μA, and field of view 90 mm. CT images were analytically reconstructed using the filtered back projection reconstruction software of the scanner (Cobra Version 7.3.4, Exxim Computing Corporation, Pleasanton, CA, USA) into a 256 × 256 × 512 matrix with 200 μm isotropic voxel size. Each resultant CT image was inherently co-registered with the corresponding PET scan.

Image analysis was performed using AMIDE imaging software. For quantification of the PET signal, regions of interest (ROIs) were drawn at the level of the ascending aorta and aortic arch (region with most extensive atherosclerotic lesion development) based on anatomical CT imaging. Mean standardized uptake values (SUV) were used to compare aortic uptake.

Statistical analysis

Data are expressed as mean ± standard deviation. Variables were tested for homogeneity of variance by the Levene test. Comparisons between groups were performed using the one-way ANOVA tests with corrections for multiple comparisons. Correlations between variables were evaluated using the Spearman correlation coefficient. A P-value of <0.05 was considered significant. Statistical analysis was done using SPSS Statistics software (version 22.0.0, IBM Company, Chicago, IL, USA).

Results

^{18}F -Radiolabelling of cAbVCAM-1–5 nanobody

As direct ^{18}F-fluorination methods of proteins are difficult, the first step in ^{18}F-radiolabelling of cAbVCAM-1–5 Nb was the synthesis of the prosthetic group [^{18}F]-SFB. [^{18}F]-SFB was radiosynthesized and purified with 55 ± 5% yield and a radiochemical purity of >95%. After the radiolabeling reaction with cAbVCAM-1–5 Nb and purification, [^{18}F]FB-anti-VCAM-1 Nb was obtained with a radiochemical purity of >99% (*Figure 1A* and *B*). The chemical identity of [^{18}F]FB-cAbVCAMb1–5 was confirmed by comparison of the gamma-trace with the UV-profile of the non-radioactive cAbVCAM-1–5 Nb on RP-HPLC. The radiolabelled compound was stable in PBS over a period of at least 3 h with >98% intact [^{18}F]FB-cAbVCAM-1–5 Nb (*Figure 1C*). Both *in vitro* and *in vivo*, the ^{18}F-labelled Nb showed minimal binding to serum proteins and was not degraded (*Figure 1D* and *E*). Conversely, [^{18}F]FB-cAbVCAM-1–5 was metabolized in the kidneys, and metabolites are excreted in the urine (*Figure 1F*).

In vitro assessment of functionality and specificity

To assess the functionality and specificity of [^{18}F]FB-cAbVCAM-1–5, cell-binding studies on VCAM-1 expressing bEND5 cells and VCAM-1-negative bEND5 cells were performed. To demonstrate that the binding was receptor-specific, a 300-fold excess of unlabelled cAbVCAM-1–5 Nb was added to VCAM-1-positive cells. The results showed that the binding of [^{18}F]FB-cAbVCAM-1–5 was receptor-mediated and could be inhibited by receptor saturation (*Figure 2*).

Biodistribution

A summary of the biodistribution data for [^{18}F]FB-cAbVCAM-1–5 in ApoE$^{-/-}$ and C57Bl/6 mice at 3 h post-injection is presented in *Table 1*. These data show that ^{18}F-labelled Nbs were rapidly cleared from circulation due to their fast renal clearance. An uptake of <0.5% ID/g was observed in all other tissues and organs, except for the spleen (1.76 ± 0.76 and 1.88 ± 0.34%ID/g in ApoE$^{-/-}$ and C57Bl/6, respectively), an organ known to express VCAM-1 constitutively.[10] This splenic uptake was not observed in the presence of an excess of cold cAbVCAM-1–5 or for [^{18}F]FB-cAbBCII10.

Uptake in atherosclerotic lesions

In ApoE$^{-/-}$ mice, [^{18}F]FB-cAbVCAM-1–5 uptake in excised aorta segments with Score 1 (1.18 ± 0.36%ID/g), Score 2 (1.49 ± 0.37%ID/g) and 3 (1.61 ± 0.41%ID/g) was significantly higher compared with segments with Score 0 (0.68 ± 0.16%ID/g, $P = 0.001$), compared with the uptake in aorta segments of control mice (0.52 ± 0.20%ID/g, $P < 0.0001$), and compared with the uptake of the non-targeting [^{18}F]FB-cAbBCII10 Nb in segments of all scores (Score 3: 0.33 ± 0.09%ID/g, $P < 0.0001$) ((*Figure 3*). Co-injection of a 70-fold excess of unlabelled cAbVCAM-1–5 Nb in ApoE$^{-/-}$ mice resulted in a significant decrease in aortic uptake to the baseline level (Score 3: 0.78 ± 0.27%ID/g, $P = 0.001$) (*Figure 3*). Moreover, [^{18}F]FB-cAbVCAM-1–5 uptake in aorta segments of ApoE$^{-/-}$ mice correlated with the lesion-extension index (Spearman's $r^2 = 0.675$, $P < 0.0001$). Fast blood clearance and low myocardial uptake of the Nb resulted in high lesion-to-blood, lesion-to-heart, and lesion-to-control vessel ratios (3.3 ± 0.4, 12.4 ± 0.4, and 3.1 ± 0.6, respectively).

PET/CT imaging

In accordance with the *ex vivo* biodistribution data, PET/CT images revealed for both ^{18}F-labelled Nbs high signals in the kidneys and the bladder. Signals in other organs and tissues were very low. Analysis of transversal, coronal, and sagittal PET/CT images showed accumulation of [^{18}F]FB-cAbVCAM-1–5 at the level of ascending aorta and aortic arch of ApoE$^{-/-}$ mice, the region where most of the segments are scored as 3, while only background signals were observed for the control groups (*Figure 4A*). Hence, quantification of the mean SUV in this region revealed this difference was significant ($P < 0.0001$) (*Figure 4B*). Lesions along the abdominal aorta could not be identified due to the high renal activity.

Downloaded from by guest on January 26, 2016

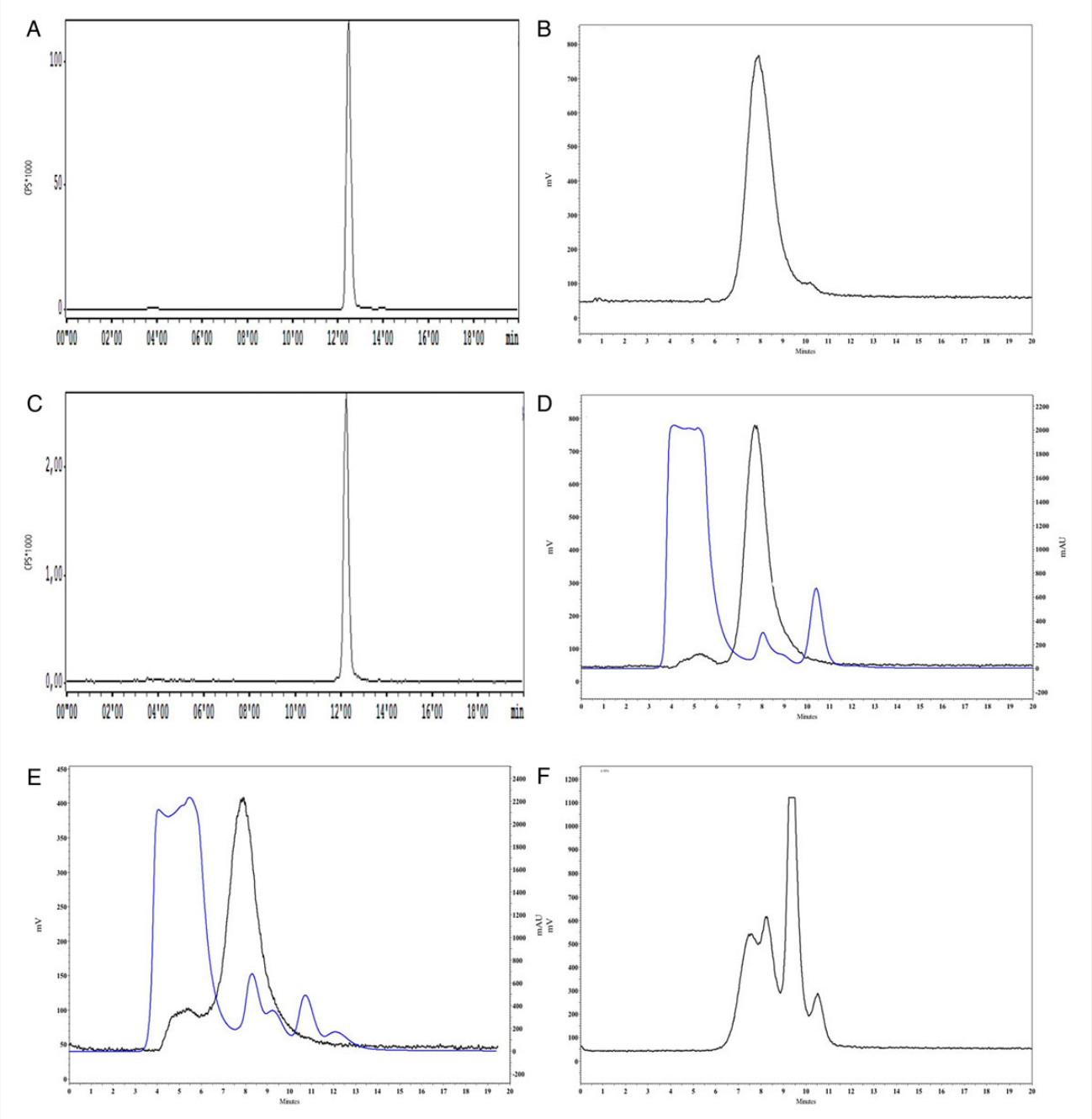

Figure 1 Evaluation of radiochemical purity, stability and metabolization of the [^{18}F]FB-cAbVCAM-1–5 tracer by RP-HPLC analysis (*A* and *C*) and SEC analysis (*B* and *D*–*F*). (*A* and *B*) [^{18}F]FB-cAbVCAM-1–5 elutes as a single peak without the presence of free ^{18}F or unreacted ^{18}F-SFB [gamma-trace, t_R = 12.5 (RP-HPLC) and 8 min (SEC)]. (*C* and *D*) *In vitro* stability of [^{18}F]FB-cAbVCAM-1–5 after 3 h, respectively, in PBS (>98%) and serum (>98%). (*E*) *In vivo* stability in serum 5 min after injection. (*F*) Urine sample 30 min after injection showing metabolization of [^{18}F]FB-cAbVCAM-1–5. (Blue: Absorbance at 280 nm representing serum proteins, black: radioactive signal.)

Discussion

In the present study, we have described the development and validation of a new PET tracer specific for VCAM-1, and we demonstrated the non-invasive PET/CT imaging of VCAM-1 expression in atherosclerotic plaques in a murine model. This may represent an attractive tool for clinical translation of imaging inflamed atherosclerotic plaques in patients.

Recently, we have reported the selection of the lead compound cAbVCAM-1–5 with nanomolar affinity for mouse and human VCAM-1 based on the screening of 10 Nbs derived from heavy-chain-only antibodies raised in an immunized dromedary.[10]

Downloaded from by guest on January 26, 2016

This compound was labelled with ^{99m}Tc for SPECT imaging of atherosclerotic lesions in ApoE$^{-/-}$ mice and it was shown that the uptake of ^{99m}Tc-cAbVCAM-1–5 correlated with the level of VCAM-1 expression in these lesions.[11] Moreover, SPECT/CT imaging with this tracer was used to monitor the anti-inflammatory effects of statins.[11] In the current study, cAbVCAM-1–5 Nb was radiolabelled with ^{18}F, often referred to as the 'radionuclide of choice' for PET imaging. Compared with other imaging modalities, PET is currently the preferred clinical modality because it is the most sensitive and quantitative clinical molecular imaging technology. This feature is particularly important for the detection of molecular markers of atherosclerotic plaques where targets are commonly small and sparse.

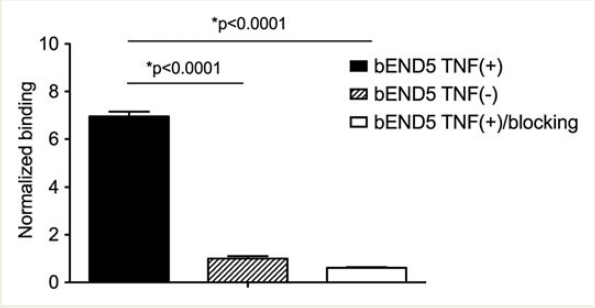

Figure 2 *In vitro* cell-binding studies. Specific binding of 5 nM [^{18}F]FB-cAbVCAM-1–5 Nb to VCAM-1 positive, TNF-α stimulated bEND5 cells. This binding was significantly higher than binding to non-stimulated cells and it was specific, as it could be blocked by an excess of unlabelled Nb. Data are presented as mean ± SD. *$P < 0.0001$ TNF-α stimulated bEND5 cells vs. non-stimulated cells and vs. blocking condition

Essential characteristics of a radiotracer for clinical translation are purity and stability, high specificity and affinity for the target, and fast blood clearance to reach high target-to-background ratios. ^{18}F-radiolabelled cAbVCAM-1–5 Nb was obtained with high radiochemical purity and remained stable and functional, both *in vitro* and *in vivo*. Atherosclerotic lesions located in the region of the ascending aorta and aortic arch of ApoE$^{-/-}$ mice were specifically identified by PET/CT imaging. To assure minimal background values in tissues such as blood and myocardium, imaging was performed at 2–3 h after injection, a time frame feasible for ^{18}F-labelled probes. These findings make the [^{18}F]FB-cAbVCAM-1–5 Nb a quite attractive tracer for human imaging.

Nanobodies labelled with radiometals such as ^{99m}Tc typically show intense kidney retention in the proximal tubuli of the kidney

Table 1 ***Ex-vivo*** **biodistribution data of [^{18}F]-FB-cAbVCAM-1–5 and [^{18}F]-FB-cAbBCII-10 Nb 3 h after injection in C57Bl/6 and ApoE$^{-/-}$ mice**

	^{18}F-cAbVCAM-1–5		^{18}F-cAbVCAM-1–5/ blocking	^{18}F-cAbBCII-10	*P*-values
	ApoE$^{-/-}$	C57Bl/6	ApoE$^{-/-}$	ApoE$^{-/-}$	
Blood	0.48 ± 0.20	0.41 ± 0.03	0.52 ± 0.17	0.31 ± 0.16	NS
Liver	0.39 ± 0.16[a,b]	0.28 ± 0.03	0.22 ± 0.06	0.13 ± 0.03	[a]$P = 0.048$ [b]$P = 0.010$
Spleen	1.76 ± 0.76[a,b]	1.88 ± 0.34	0.47 ± 0.06	0.11 ± 0.03	[a]$P = 0.009$ [b]$P = 0.003$
Pancreas	0.17 ± 0.07	0.14 ± 0.13	0.16 ± 0.04	0.18 ± 0.06	NS
Kidneys	27.84 ± 12.83[b,c]	3.33 ± 0.74	21.52 ± 6.3	40.64 ± 15.90	[c]$P < 0.0001$ [b]$P = 0.042$
Stomach	0.22 ± 0.12	0.13 ± 0.03	0.18 ± 0.07	0.25 ± 0.17	NS
Small intestines	0.21 ± 0.11	0.19 ± 0.05	0.14 ± 0.04	0.14 ± 0.11	NS
Large intestines	0.17 ± 0.07	0.13 ± 0.05	0.13 ± 0.02	0.09 ± 0.03	NS
Heart	0.13 ± 0.04	0.18 ± 0.05	0.13 ± 0.03	0.09 ± 0.03	NS
Lungs	0.44 ± 0.30[b]	0.60 ± 0.18	0.39 ± 0.11	0.20 ± 0.07	[b]$P = 0.038$
Thymus	0.28 ± 0.08[a,b,c]	0.19 ± 0.05	0.17 ± 0.07	0.11 ± 0.03	[c]$P = 0.021$ [a]$P = 0.004$ [b]$P < 0.0001$
Muscle	0.08 ± 0.05	0.07 ± 0.03	0.07 ± 0.02	0.06 ± 0.04	NS
Bone	0.19 ± 0.07[b]	0.22 ± 0.06	0.16 ± 0.06	0.13 ± 0.06	[b]$P = 0.04$
Lymph nodes	0.27 ± 0.10[a,b]	0.19 ± 0.06	0.16 ± 0.06	0.13 ± 0.06	[a]$P = 0.016$ [b]$P = 0.003$
Salivary gland	0.16 ± 0.10	0.13 ± 0.03	0.12 ± 0.03	0.08 ± 0.03	NS
Fat	0.08 ± 0.05	0.08 ± 0.05	0.12 ± 0.04	0.07 ± 0.06	NS

Data are expressed as mean %ID/g ± SD.
[a]^{18}F-cAbVCAM-1–5 in ApoE$^{-/-}$ vs. ^{18}F-cAbVCAM-1–5/ blocking in ApoE$^{-/-}$.
[b]^{18}F-cAbVCAM-1–5 in ApoE$^{-/-}$ vs. ^{18}F-cAbBCII-10 in ApoE$^{-/-}$.
[c]^{18}F-cAbVCAM-1–5 in ApoE$^{-/-}$ vs. ^{18}F-cAbVCAM-1–5 in C57Bl/6.

Downloaded from by guest on January 26, 2016

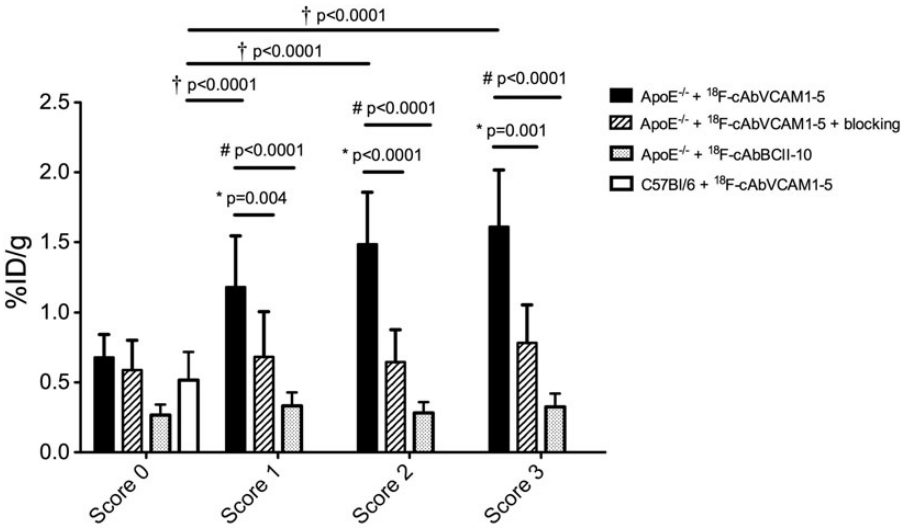

Figure 3 Uptake in aorta segments according to the lesion-extension score. Aortic uptake in ApoE$^{-/-}$ mice ($n = 6$) injected with [^{18}F]FB-cAbVCAM-1–5 ($n = 6$), [^{18}F]FB-cAbVCAM-1–5 + blocking ($n = 6$) and [^{18}F]-FB-cAbBCII-10 ($n = 6$) Nb and in C57Bl/6 mice ($n = 6$) injected with [^{18}F]-FB-cAbVCAM-1–5. Uptake of [^{18}F]FB-cAbVCAM-1–5 vs. blocking (*), vs. control Nb ($^{\#}$) and vs. aorta control mice (†).

cortex by a mechanism that is at least partially mediated by the megalin-receptor system.[24] Remarkably, the kidney retention of [^{18}F]FB-cAbVCAM-1–5 was much lower compared with ^{99m}Tc-cAbVCAM-1–5 Nb (27.84 ± 12.83 vs. 222 ± 12%ID/g). This can be explained by renal metabolization of the ^{18}F-labelled tracer and excretion of the metabolites via the urine. Furthermore, a higher uptake of ^{99m}Tc-cAbVCAM-1–5 Nb is observed in organs with constitutive VCAM-1 expression such as spleen, thymus, lymph nodes, and bone marrow, compared with [^{18}F]FB-cAbVCAM-1–5 [e.g. spleen (1.76 ± 0.76 vs. 9.2 ± 1.0%ID/g), thymus (0.28 ± 0.08 vs. 1.7 ± 0.1% ID/g)]. We speculate that these differences are partly due to different specific activities of the tracers next to different biophysical and chemical properties of the radiolabelled compounds *in vivo*. Nevertheless, comparable lesion-to-blood and lesion-to-heart ratios were observed.

The abundant presence of macrophages is a hallmark feature of potential vulnerable plaques.[25] Over the past decade, there has been increasing interest in the development of molecular imaging methods capable of imaging the extent of plaque inflammation that could potentially provide powerful predictive information on future cardiovascular events.[26] VCAM-1 expression has been most preferentially studied because of its function to recruit inflammatory cells to the arterial intima and because its expression pattern could reflect the degree of plaque inflammation.[6] Indeed, several molecular imaging strategies targeting VCAM-1 in the context of atherosclerosis have been demonstrated using ultrasound,[27,28] magnetic resonance,[29] optica,l[30] or nuclear imaging.[10,31] To this purpose, Nahrendorf *et al.* have previously developed a multimeric peptide-based tracer, ^{18}F-4V, for PET/CT imaging of VCAM-1 expression. Comparable results with the present study were obtained in terms of lesion-to-normal vessels, lesion-to-blood, and lesion-to-myocardium ratios.

Besides the anti-VCAM-1 Nb presented in this study, many other Nb-based tracers have been developed and validated in preclinical models for the imaging of a variety of specific disease-related biomarkers.[32] They have been successfully labelled with different radioisotopes (^{68}Ga, ^{99m}Tc, ^{18}F, ^{111}In),[12,33] near infrared dyes,[34] microbubbles,[35] or gadolinium vesicles[36] allowing their use for multiple imaging modalities such as SPECT, PET, optical imaging, ultrasound, or MRI. The Nb technology represents thus a versatile tool for molecular imaging with great potential for clinical applications. Hence, a Phase I clinical trial has been finalized successfully regarding the application of a ^{68}Ga-labelled HER2-specific Nb as PET tracer to screen breast cancer patients for HER2 expression.[17] Moreover, preparations for a Phase I clinical trial with cAbVCAM-1–5 Nb have already been initiated as the current tracer is being produced complying with Good Manufacturing Practice (GMP) requirements.

In clinical research ^{18}F-FDG has been widely used for imaging of plaque inflammation in carotid lesions.[37] However, coronary artery imaging remains extremely challenging due to high myocardial background that is generally greater than any signal originating from a plaque. The low myocardial uptake of [^{18}F]FB-cAbVCAM-1–5 Nb with a high lesion-to-myocardium ratio renders it a promising tracer for potential molecular imaging of coronary atherosclerosis in patients. Indeed, the feasibility of coronary molecular imaging in patients using PET/CT has already been shown using ^{18}F-sodium fluoride (^{18}F-NaF) as a tracer of active microcalcification in atherosclerotic plaques[38] or ^{18}F-FLT, a thymine analogue accumulating in proliferating cells.[20] However, further studies are needed to evaluate the impact of these findings on patient management and treatment.

Study limitations

The present approach of PET/CT imaging of VCAM-1 expression requests some considerations. The majority of thrombotic events in culprit lesions are caused by plaque rupture.[25] These plaques show typically intensive infiltration of inflammatory cells. However,

Downloaded from by guest on January 26, 2016

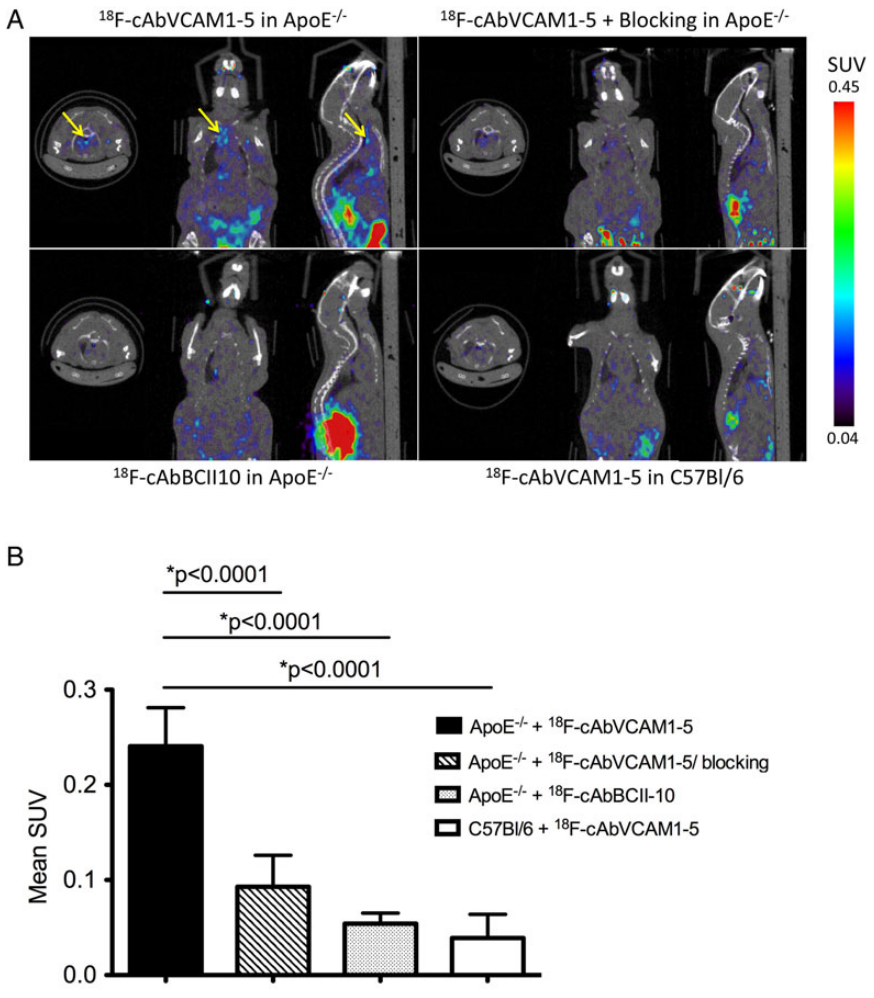

Figure 4 PET/CT imaging in ApoE$^{-/-}$ and C57Bl/6 mice. (*A*) Representative PET/CT images of ApoE$^{-/-}$ and C57Bl/6 mice 2–3 h after injection of the radiotracer. Focal uptake of [^{18}F]-FB-cAbVCAM-1–5 Nb is visible at the level of the ascending aorta and aortic arch in ApoE$^{-/-}$ mice, while background uptake is observed in C57Bl/6 control mice and in ApoE$^{-/-}$ mice injected with control Nb. This focal uptake is specific as it could be blocked by an excess of unlabelled Nb. (*B*) Quantification of PET signal at the level of aortic arch as the mean SUV ($n = 3$ per group). Data expressed as mean ± SD. *$P < 0.0001$ [^{18}F]-FB-cAbVCAM-1–5 in ApoE$^{-/-}$ mice vs. blocking experiments, vs. control Nb and vs. control animals.

20–30% of coronary thrombi evolve from plaques that do not have a large lipid core or significant inflammation but have superficial endothelial erosions.[3] This subset of high-risk plaques might be missed by the current method.

In this study, we were able to visualize plaque inflammation in a murine model of atherosclerosis. However, atherosclerotic lesions of murine models differ from human pathology. [^{18}F]FB-cAbVCAM-1–5 Nb imaging of plaque inflammation in human coronary and carotid arteries remains to be further investigated.

Conclusion

The present study demonstrates a sensitive and specific method for non-invasive PET/CT imaging of VCAM-1 expression within atherosclerotic lesions, which may provide important information to characterize atherosclerotic plaque inflammation. This preclinical validation study holds the potential to be translated in patients. Further clinical studies are needed to put this technology a step forward in our quest for imaging potential vulnerable plaques.

Supplementary data

Supplementary data are available at *European Heart Journal – Cardiovascular Imaging* online.

Acknowledgments

Authors thank Cindy Peleman for technical assistance.

Conflict of interest: None declared.

Funding

This research has been supported by a grant of Research Foundation—Flanders (FWO) and Scientific Fund Willy Gepts, UZ Brussel.

Downloaded from by guest on January 26, 2016

References

1. Libby P, Ridker PM. Inflammation and atherothrombosis: from population biology and bench research to clinical practice. *J Am Coll Cardiol* 2006;**48**(9, Suppl.):A33–46.
2. Libby P. Inflammation in atherosclerosis. *Nature* 2002;**420**:868–74.
3. Virmani R, Burke AP, Farb A, Kolodgie FD. Pathology of the vulnerable plaque. *J Am Coll Cardiol* 2006;**47**(8, Suppl.):C13–8.
4. Cybulsky MI, Iiyama K, Li H, Zhu S, Chen M, Iiyama M *et al.* A major role for VCAM-1, but not ICAM-1, in early atherosclerosis. *J Clin Invest* 2001;**107**:1255–62.
5. Obrien KD, Allen MD, Mcdonald TO, Chait A, Harlan JM, Fishbein D *et al.* Vascular cell-adhesion molecule-1 is expressed in human coronary atherosclerotic plaques—implications for the mode of progression of advanced coronary atherosclerosis. *J Clin Invest* 1993;**92**:945–51.
6. Nahrendorf M, McCarthy JR, Libby P. Over a hump for imaging atherosclerosis: nanobodies visualize vascular cell adhesion molecule-1 in inflamed plaque. *Circ Res* 2012;**110**:902–3.
7. Hamers-Casterman C, Atarhouch T, Muyldermans S, Robinson G, Hammers C, Songa EB *et al.* Naturally occurring antibodies devoid of light chains. *Nature* 1993;**363**:446–8.
8. Vaneycken I, D'huyvetter M, Hernot S, De Vos J, Xavier C, Devoogdt N *et al.* Immuno-imaging using nanobodies. *Curr Opin Biotechnol* 2011;**22**:877–81.
9. Vaneycken I, Devoogdt N, Van Gassen N, Vincke C, Xavier C, Wernery U *et al.* Preclinical screening of anti-HER2 nanobodies for molecular imaging of breast cancer. *FASEB J* 2011;**25**:2433–46.
10. Broisat A, Hernot S, Toczek J, De Vos J, Riou LM, Martin S *et al.* Nanobodies targeting mouse/human VCAM1 for the nuclear imaging of atherosclerotic lesions. *Circ Res* 2012;**110**:927–37.
11. Broisat A, Toczek J, Dumas LS, Ahmadi M, Bacot S, Perret P *et al.* 99mTc-cAbVCAM1-5 imaging is a sensitive and reproducible tool for the detection of inflamed atherosclerotic lesions in mice. *J Nucl Med* 2014;**55**:1678–84.
12. Xavier C, Vaneycken I, D'huyvetter M, Heemskerk J, Keyaerts M, Vincke C *et al.* Synthesis, preclinical validation, dosimetry, and toxicity of 68Ga-NOTA-anti-HER2 nanobodies for iPET imaging of HER2 receptor expression in cancer. *J Nucl Med* 2013;**54**:776–84.
13. Zheng F, Devoogdt N, Sparkes A, Morias Y, Abels C, Stijlemans B *et al.* Monitoring liver macrophages using nanobodies targeting Vsig4: concanavalin A induced acute hepatitis as paradigm. *Immunobiology* 2015;**220**:200–9.
14. Zheng F, Put S, Bouwens L, Lahoutte T, Matthys P, Muyldermans S *et al.* Molecular imaging with macrophage CRIg-targeting nanobodies for early and preclinical diagnosis in a mouse model of rheumatoid arthritis. *J Nucl Med* 2014;**55**:824–9.
15. Put S, Schoonooghe S, Devoogdt N, Schurgers E, Avau A, Mitera T *et al.* SPECT imaging of joint inflammation with nanobodies targeting the macrophage mannose receptor in a mouse model for rheumatoid arthritis. *J Nucl Med* 2013;**54**:807–14.
16. De Vos J, Devoogdt N, Lahoutte T, Muyldermans S. Camelid single-domain antibody-fragment engineering for (pre)clinical in vivo molecular imaging applications: adjusting the bullet to its target. *Expert Opin Biol Ther* 2013;**13**:1149–60.
17. Keyaerts M, Xavier C, Heemskerk J, Devoogdt N, Everaert H, Ackaert C *et al.* Phase I study of 68Ga-HER2-nanobody for PET/CT assessment of HER2-expression in breast carcinoma. *J Nucl Med* 2016;**57**:27–33.
18. Bala G, Cosyns B. Recent advances in visualizing vulnerable plaque: focus on non-invasive molecular imaging. *Curr Cardiol Rep* 2014;**16**:520.
19. Gaemperli O, Shalhoub J, Owen DRJ, Lamare F, Johansson S, Fouladi N *et al.* Imaging intraplaque inflammation in carotid atherosclerosis with 11C-PK11195 positron emission tomography/computed tomography. *Eur Heart J* 2012;**33**:1902–10.
20. Ye Y-X, Calcagno C, Binderup T, Courties G, Keliher EJ, Wojtkiewicz GR *et al.* Imaging macrophage and hematopoietic progenitor proliferation in atherosclerosis. *Circ Res* 2015;**117**:835–45.
21. Rosenbaum D, Millon A, Fayad Z. Molecular imaging in atherosclerosis: FDG PET. *Curr Atheroscler Rep* 2012;**14**:429–37.
22. Hirvonen J, Roivainen A, Virta J, Helin S, Någren K, Rinne J. Human biodistribution and radiation dosimetry of 11C-(R)-PK11195, the prototypic PET ligand to image inflammation. *Eur J Nucl Med Mol Imaging* 2010;**37**:606–12.
23. Blykers A, Schoonooghe S, Xavier C, D'hoe K, Laoui D, D'Huyvetter M *et al.* PET imaging of macrophage mannose receptor–expressing macrophages in tumor stroma using 18F-radiolabeled camelid single-domain antibody fragments. *J Nucl Med* 2015;**56**:1265–71.
24. Tchouate Gainkam LO, Caveliers V, Devoogdt N, Vanhove C, Xavier C, Boerman O *et al.* Localization, mechanism and reduction of renal retention of technetium-99m labeled epidermal growth factor receptor-specific nanobody in mice. *Contrast Media Mol Imaging* 2011;**6**:85–92.
25. Naghavi M, Libby P, Falk E, Casscells SW, Litovsky S, Rumberger J *et al.* From vulnerable plaque to vulnerable patient: a call for new definitions and risk assessment strategies: Part I. *Circulation* 2003;**108**:1664–72.
26. Rudd JH, Fayad ZA. Imaging atherosclerotic plaque inflammation. *Nat Clin Pract Cardiovasc Med* 2008;**5**(Suppl. 2):S11–7.
27. Hamilton AJ, Huang S-L, Warnick D, Rabbat M, Kane B, Nagaraj A *et al.* Intravascular ultrasound molecular imaging of atheroma components in vivo. *J Am Coll Cardiol* 2004;**43**:453–60.
28. Kaufmann BA, Sanders JM, Davis C, Xie A, Aldred P, Sarembock IJ *et al.* Molecular imaging of inflammation in atherosclerosis with targeted ultrasound detection of vascular cell adhesion molecule-1. *Circulation* 2007;**116**:276–84.
29. McAteer MA, Schneider JE, Ali ZA, Warrick N, Bursill CA, von zur Muhlen C *et al.* Magnetic resonance imaging of endothelial adhesion molecules in mouse atherosclerosis using dual-targeted microparticles of iron oxide. *Arterioscler Thromb Vasc Biol* 2008;**28**:77–83.
30. Kelly KA, Allport JR, Tsourkas A, Shinde-Patil VR, Josephson L, Weissleder R. Detection of vascular adhesion molecule-1 expression using a novel multimodal nanoparticle. *Circ Res* 2005;**96**:327–36.
31. Dimastromatteo J, Broisat A, Perret P, Ahmadi M, Boturyn D, Dumy P *et al.* In vivo molecular imaging of atherosclerotic lesions in ApoE−/− mice using VCAM-1–specific, 99mTc-labeled peptidic sequences. *J Nucl Med* 2013;**54**:1442–9.
32. Chakravarty R, Goel S, Cai W. Nanobody: the "magic bullet" for molecular imaging? *Theranostics* 2014;**4**:386–98.
33. Xavier C, Devoogdt N, Hernot S, Vaneycken I, D'Huyvetter M, De Vos J *et al.* Site-specific labeling of his-tagged nanobodies with 99mTc: a practical guide. In: Saerens D, Muyldermans S, eds. *Single Domain Antibodies. Methods in Molecular Biology*. Vol. 911. Humana Press; 2012. p485–90.
34. Kijanka M, Warnders F-J, El Khattabi M, Lub-de Hooge M, van Dam G, Ntziachristos V *et al.* Rapid optical imaging of human breast tumour xenografts using anti-HER2 VHHs site-directly conjugated to IRDye 800CW for image-guided surgery. *Eur J Nucl Med Mol Imaging* 2013;**40**:1718–29.
35. Hernot S, Unnikrishnan S, Du Z, Shevchenko T, Cosyns B, Broisat A *et al.* Nanobody-coupled microbubbles as novel molecular tracer. *J Control Release* 2012;**158**:346–53.
36. Iqbal U, Albaghdadi H, Nieh MP, Tuor UI, Mester Z, Stanimirovic D *et al.* Small unilamellar vesicles: a platform technology for molecular imaging of brain tumors. *Nanotechnology* 2011;**22**:195102.
37. Tarkin JM, Joshi FR, Rudd JHF. PET imaging of inflammation in atherosclerosis. *Nat Rev Cardiol* 2014;**11**:443–57.
38. Joshi NV, Vesey AT, Williams MC, Shah ASV, Calvert PA, Craighead FHM *et al.* 18F-fluoride positron emission tomography for identification of ruptured and high-risk coronary atherosclerotic plaques: a prospective clinical trial. *Lancet* 2014;**383**:705–13.

Downloaded from by guest on January 26, 2016